JOURNAL OF MATERIALS SCIENCE 27 (1992) 1385 – 1390

Deformation mechanisms during uniaxial drawing of melt-crystallized ultra-high molecular weight polyethylene

N.S.J.A. GERRITS
Department of Materials Technology, DSM Research, PO Box 18, 6160 MD Geleen, The Netherlands

Y.TERVOORT
Department of Polymer Technology, Eindhoven University of Technology, PO Box 513, 5600 MB Eindhoven, The Netherlands

The crystal deformation mechanisms during solid-state uniaxial drawing of melt-crystallized ultra-high molecular weight polyethylene (UHMW-PE) film have been studied as a function of draw ratio. At higher draw ratios ($\lambda \geq 3$) the fine slip processes during uniaxial drawing of melt-crystallized UHMW-PE result in a single-crystal-like (1 0 0) [0 0 1] texture, whereas the normals to the lamellae are inclined by more than 45° with respect to the applied force. It is postulated that in melt-crystallized UHMW-PE the coarse slip process is predominantly restricted due to the fold plane restraints, preventing lamellae from breaking up and rotating with their normals towards the draw direction. The inclination of lamellar normals with respect to the draw direction prohibits further drawing because shear stresses act perpendicular instead of parallel to the lamellar normals.

1. Introduction

The deformation processes during solid-state uniaxial drawing or roller drawing of polyethylene have been extensively discussed based on the detailed data of the morphology and the properties of drawn materials [1–6]. Most of the experimental results currently available support the deformation processes originally proposed by Peterlin and co-workers [2, 4–6] for drawing of melt-crystallized normal molecular weight polyethylene. In the initial stages of drawing, both the chain axes and the normals to the lamellae rotate towards the draw direction. This is followed by crystal breakdown resulting in the formation of microfibrils. Further deformation leads to shearing of microfibrils, a process limited by interfibrillar tie molecules [6].

The deformation processes during solid-state drawing of melt-crystallized ultra-high molecular weight polyethylene (UHMW-PE) have been studied by Yoda and Kuriyama [7], Kaito *et al.* [8, 9], van Aerle and Braam [10]. They concluded that for the maximum attainable draw ratio of approximately 5, the chain axes are oriented parallel to the draw direction, but the normals to the lamellae are inclined to the draw direction.

In contrast to melt-crystallized UHMW-PE, deformation of solution-crystallized UHMW-PE films [11, 12] can result in an orientation of both the chain axes and the normals to the lamellae parallel to the draw direction for a draw ratio above 5. Van Aerle and Braam [12] showed the initial deformation processes of solution-crystallized UHMW-PE to be basically identical to those reported by Peterlin [6] for conventional polyethylene. On further drawing of solution-crystallized UHMW-PE, the microfibrillar folded-chain crystals gradually unfold and transform into chain-extended crystals [12].

The strongly-enhanced drawability of UHMW-PE crystallized from a solution was originally proposed to be due to a reduction in the concentration of "trapped entanglements" on the basis of the relationship between the initial polymer concentration in solution and the maximum drawability of the UHMW-PE films [13]. However, ultra-drawability is completely lost by heating the material above its melting point for a short period of time (1 min, 142 °C) [14]. On the other hand, it is rapidly regained once the system is heated in the presence of solvent above the dissolution temperature [14]. Because of the high rate of transformation from a draw-resistant into an ultra-drawable material and vice versa, Lemstra *et al.* [14] have suggested that in addition to trapped entanglements the local arrangement of chain segments may drastically modulate the drawability.

In order to specify the nature of constraints governing the solid-state drawability the deformation mechanisms during uniaxial drawing of melt-crystallized UHMW-PE are interpreted from considerations of crystal plasticity and deformation in the amorphous

0022–2461 © *1992 Chapman & Hall*

phase. Normal uniaxial drawing produces specimens with a fibre texture which does not provide a good insight into the deformation mechanisms. Therefore, uniaxial drawing of UHMW-PE films constrained at constant width has been employed resulting in a three-dimensional crystallite orientation.

2. Experimental procedure

2.1. Sample preparation

In order to obtain homogeneous melt-crystallized UHMW-PE films, solution-crystallized UHMW-PE films were used as a starting material. These films were prepared by continuously extruding a 15% solution of UHMW-PE (Himont HB312 CM, $M_W = 1.5 \times 10^3\ kg\,mol^{-1}$) in decalin. The solution was quenched in water and the resultant film was dried at ambient temperature. The films were melted by immersing them in silicone oil at 140 °C for 1 min and no dimensional change was observed. The melting temperature of the solution-crystallized UHMW-PE film was 133 °C as determined from DSC measurements.

The melt-crystallized UHMW-PE films were drawn uniaxially constrained at constant width using a stretching frame made by Iwamoto Seisakusho Ltd. The initial sample dimensions were $60 \times 60\ mm^2$ and a crosshead speed of $20\ mm\,s^{-1}$ and a temperature of 120 °C were employed for the drawing process. The exact draw ratios ranging between 1 and 5 were determined by measuring the displacement of ink marks, placed 1 cm apart, on the specimen prior to drawing. In this paper the draw direction will be referred to as "DD", the direction normal to the surface as "ND" and the direction in the film plane and normal to the applied force as "TD", the transverse draw direction.

2.2. X-ray diffraction

To determine the crystal orientation wide-angle X-ray scattering (WAXS) patterns obtained by a Statton camera with a flat-film geometry and nickel-filtered CuK_α radiation from a Philips PW1729 generator operated at 50 kV and 40 mA was employed. Diffraction patterns were obtained at room temperature with the incident X-ray beam both normal and parallel to the sample surface.

The average crystal sizes were obtained from the X-ray line-broadening data. Profiles of the (1 1 0) reflections were recorded using a Philips PW1820 wide-angle diffractometer employed in the transmission mode. Nickel-filtered CuK_α radiation from a Philips PW1731 generator operated at 50 kV and 40 mA was employed. Instrumental broadening was corrected for, by using an aluminium oxide standard with an integral breadth, $\Delta\beta_{inst}$, of 0.32° for a reflection at $2\theta = 25.6°$. The observed integral breadth, $\Delta\beta_{obs}$, is defined by

$$\Delta\beta_{obs} = \frac{1}{I_{max}} \int_{2\theta=20°}^{2\theta=23°} I\,(2\theta)\,\mathrm{d}\,(2\theta) \qquad (1)$$

The integral breadth of the sample, $\Delta\beta_{sample}$, was obtained from the observed integral breadth, $\Delta\beta_{obs}$, using the following equation:

$$\Delta\beta^2_{obs} = \Delta\beta^2_{sample} + \Delta\beta^2_{inst} \qquad (2)$$

Equation 2 is based on the assumption that the true line profile, the instrumental broadening and, therefore, the observed line profile are Gaussian. Because the polymer reflection profiles are nearly always broad, a pure Gaussian assumption is generally applicable [15]. The average crystal sizes along the normal to the (1 1 0) crystal plane, $D_{1\,1\,0}$, were calculated using the Scherrer equation

$$D_{1\,1\,0} = \frac{K\lambda_X}{\Delta\beta_{sample} \cos\theta_{1\,1\,0}} \qquad (3)$$

in which $2\theta_{1\,1\,0}$ is the corresponding Bragg reflection angle, $\Delta\beta_{sample}$ is the integral breadth of the sample in radians, λ_X is the wavelength of the X-ray source (0.154 nm) and K is a constant [15] taken to be 0.9.

Small-angle X-ray scattering (SAXS) patterns were determined using a Kiessig camera equipped with a very fine pinhole collimation system. Nickel-filtered CuK_α radiation generated at 50 kV and 40 mA from a Philips PW1730 generator was employed. The sample-to-film distance was 400 mm and diffraction patterns were obtained with the incident X-ray beam both normal and parallel to the sample surface.

2.3. Electron microscopy

Transmission electron microscopy was performed using a Jeol 2000 FX transmission electron microscope operated at 100 kV. Samples trimmed and embedded ready for microtoming were solution-stained with ruthenium tetroxide at room temperature for 18 h. Thin sections were obtained using an ultramicrotome (Reichert Ultracut E) at room temperature.

3. Results

Fig. 1 shows wide-angle X-ray scattering (WAXS) patterns of melt-crystallized UHMW-PE tapes recorded with the incident X-ray beam both normal and parallel to the sample surface for draw ratios varying between 1 and 5. Attempts to produce draw ratios greater than 5 resulted in premature fracture of the sample. During uniaxial drawing the chain axes tend to orient parallel to the draw direction as indicated by the sharpening of both the (1 1 0) and the (2 0 0) reflection arcs on the equator in Fig. 1a and b. The (2 0 0) planes rotate to become predominantly parallel to the sample plane as shown by the relatively high intensity of the (2 0 0) reflection in patterns recorded with the X-ray beam parallel to the sample surface (Fig. 1b). This crystal orientation with the (2 0 0) planes parallel to the sample surface and with the (0 0 1)-axis (chain axis) parallel to the direction of the applied force, is referred to as a (1 0 0) [0 0 1] texture.

Small-angle X-ray scattering (SAXS) patterns of the samples are shown in Fig. 2. The SAXS patterns are also presented schematically for clarity. The original isotropic orientation of the lamellae is transformed into four-point SAXS patterns for $\lambda \geq 3$ (Fig. 2b),

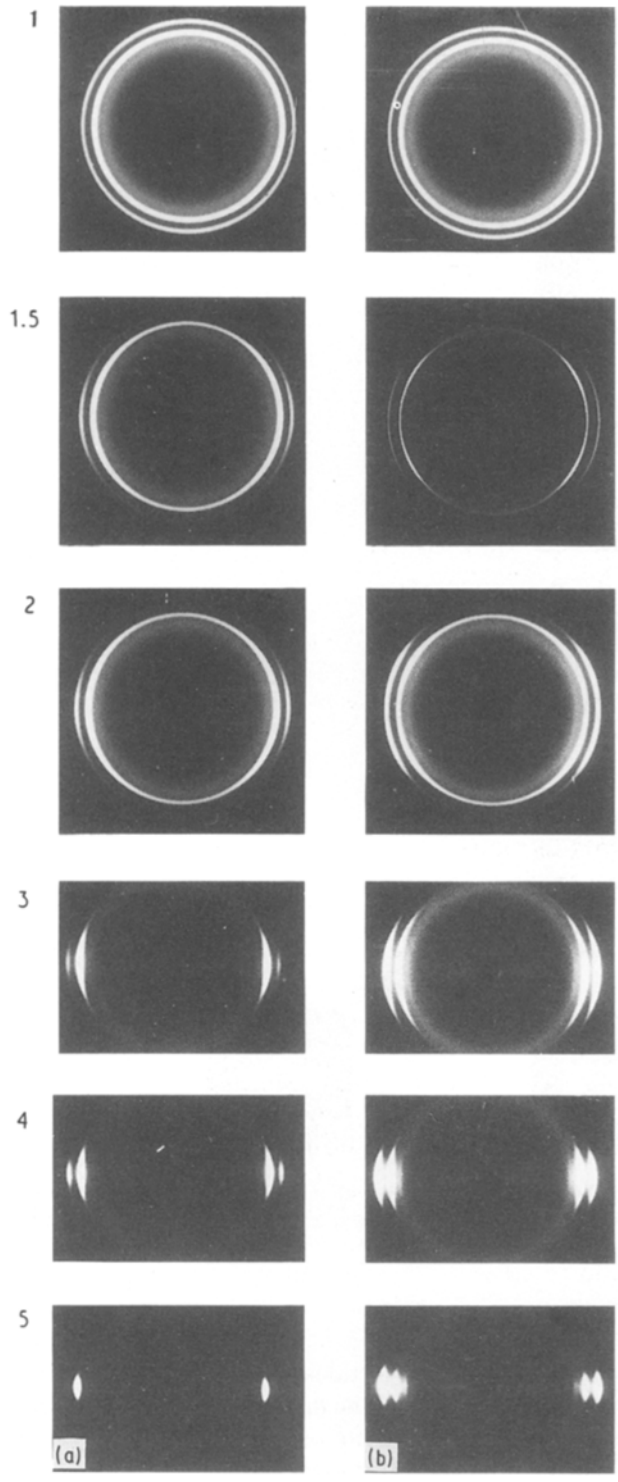

Figure 1 WAXS flat-film patterns of uniaxially-drawn melt-crystallized UHMW-PE tapes recorded with the incident X-ray beam (a) normal and (b) parallel to the sample surface. The draw direction is vertical and the draw ratio is indicated in each case.

whereas no long period can be observed if the X-ray beam is directed normal to the sample surface (Fig. 2a). The four-point pattern for $\lambda = 5$ indicates the presence of normals to the lamellae inclined by approximately 65° with respect to the draw direction. The increasing distance of the X-ray diffraction spots from the centre of the SAXS patterns (Fig. 2b) indicates a decrease in the long period with increasing draw ratio from over 30 nm to approximately 23 nm for the $\times 5$ drawn sample. This decrease cannot be related directly to a corresponding change in fold length because the initial angle between the normals to the lamellae and the chain axes is not known. Evaluation of the SAXS patterns for the $\times 5$ drawn specimen recorded with the incident X-ray beam parallel to the draw direction (Fig. 2c) indicates a long period of only 15 nm with the lamellae being well-ordered in the thickness direction of the sample.

It should be noted that real-time WAXS and SAXS measurements during drawing of melt-crystallized UHMW-PE performed by van Aerle and Braam [10], reveal a similar type of texture. Therefore, it can be concluded that the angle between the normals to the lamellae and the chain axes is not affected by relaxation during cooling from the deformation to room temperature. Fig. 3 gives a schematic representation of the morphology of a $\times 5$ drawn tape showing the relationship between the orientation of the chain axes and of the lamellar crystals.

The average lateral crystal sizes along the normal to the (1 1 0) crystal plane, $D_{1\,1\,0}$, were measured using wide-angle X-ray diffraction. $D_{1\,1\,0}$ is 35 nm for an undrawn sample and decreases continuously with increasing draw ratio to 30 nm for $\lambda = 5$. However, one should take care using the dimensions measured along the normal to the (1 1 0) reflection plane as an indication for the lateral dimensions of the lamellae. This is because the angle between the normals to the lamellae and the chain axes changes from approximately 0° to 65°.

Because the morphology is not uniquely defined by X-ray diffraction patterns, transmission electron micrographs were obtained from a $\times 5$ drawn sample. The electron micrograph from a section obtained by cutting normal to the transverse direction (Fig. 4a) reveals a lamellar type of double texture visualized in the microscope by staining the disordered interlamellar regions. From the combination of the electron micrograph and the electron diffraction pattern (Fig. 4b) it can be concluded that the normals to the lamellae are indeed inclined with respect to the chain axes, as already indicated in Fig. 3. The lamellae visualized by electron microscopy are in the same range of thickness (25–30 nm) as expected from SAXS measurements (23 nm). It should be noted that if the electron microscopy section is not exactly normal to the transverse direction both the long period and the angle between the normals to the lamellae are likely to appear to be different from their true values.

The arrangement of the lamellae can be described in several ways. At first glance a blocky pattern of relatively short lamellae is observed. From a detailed analysis of several micrographs, larger lamellae can also be observed. This becomes most pronounced if one looks for an area with a uniform intensity of the dark-grey bands originating from the stained amorphous phase. The blocky pattern can also be interpreted as a superposition of several herring-bone types of lamellar textures, which have been visualized, for example, by Grubb *et al.* [16] for room-temperature roller-drawn HDPE. However, a superposition of herring-bone patterns is not the most obvious explanation in this case, because micrographs were obtained

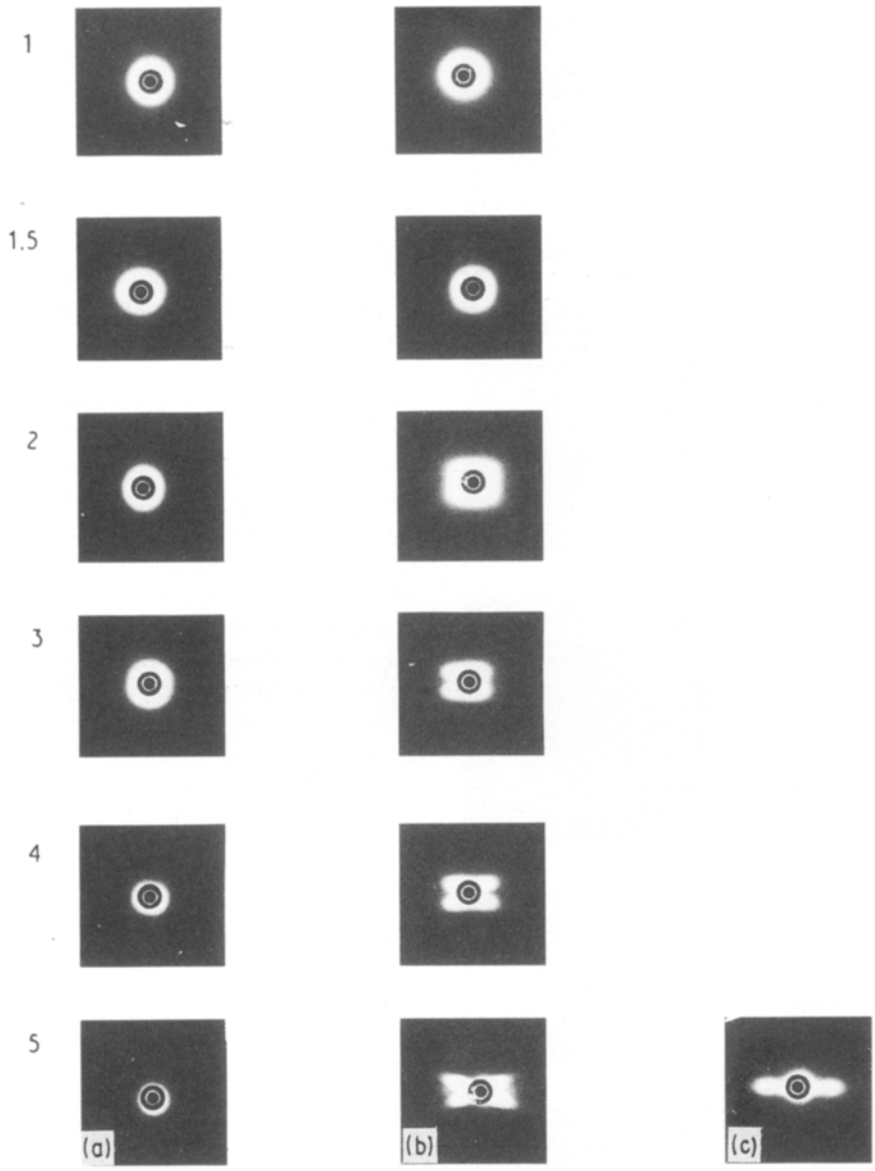

Figure 2 SAXS flat-film patterns of uniaxially-drawn melt-crystallized UHMW-PE tapes recorded with the incident X-ray beam (a) normal and (b) parallel to the sample surface and (c) with the beam parallel to the draw direction. The draw direction is vertical and the direction normal to the sample surface is horizontal. The draw ratio is indicated in each case.

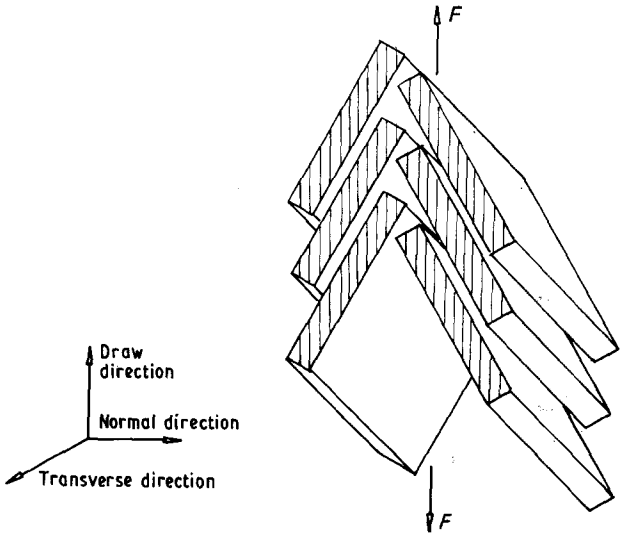

Figure 3 Schematic representation of the relationship between the orientation of the chain axes and of the lamellar crystals in a ×5 drawn melt-crystallized UHMW-PE tape.

from relatively thin sections (50 nm). Regardless of the correct description of the micrograph it is evident that the lamellae lock each other in such a way that deformation cannot proceed further.

4. Discussion

The original material ($\lambda = 1$) has an isotropic crystal orientation as can be concluded from the WAXS and SAXS patterns in Figs 1 and 2, respectively. At low draw ratios ($\lambda \leq 3$) a rotation of the chain axis parallel to the draw direction is observed from WAXS patterns. The particular slip system(s) operating will depend on the crystal orientation with respect to the applied force as shown in detail by Gerrits and Young [17]. Because the starting material is isotropic, the rotation of the chain axes is likely to be governed by a combination of chain slip and transverse slip. Initially slip occurs for crystals which are oriented such that

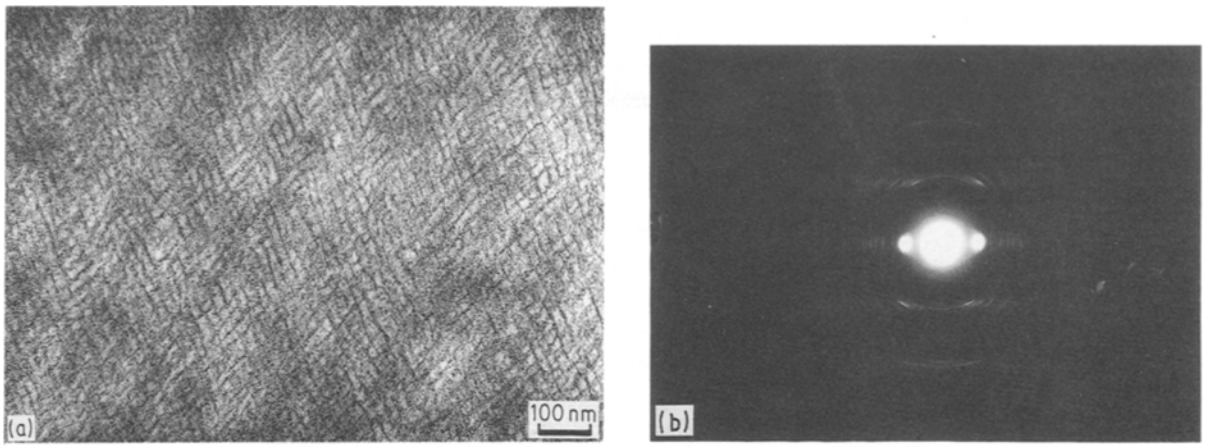

Figure 4 (a) Transmission electron micrograph of an ultramicrotomed section of a ×5 drawn melt-crystallized UHMW-PE tape. (b) The related electron diffraction pattern. The draw direction is approximately vertical.

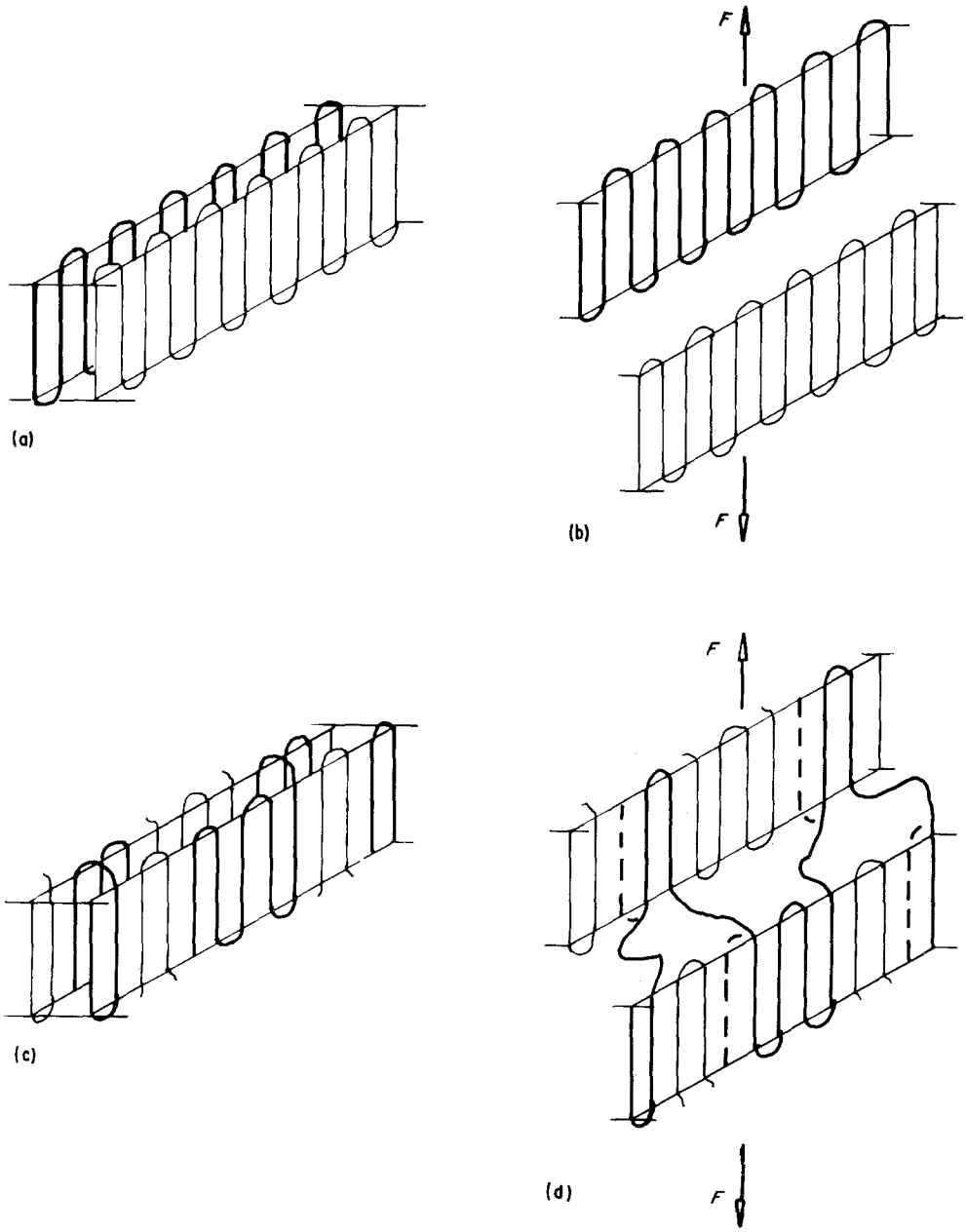

Figure 5 Schematic representation of (a) an undeformed crystal with a regular fold-plane structure, (b) as (a) but deformed by coarse slip, (c) an undeformed crystal with an irregular fold-plane structure, and (d) as (c) but deformed by coarse slip.

the critical resolved shear stress is highest on the slip planes.

At higher draw ratios ($\lambda > 3$) the slip processes result in a single-crystal-like (1 0 0) [0 0 1] texture. This type of texture has already been observed for uniaxially-drawn melt-crystallized [7–9] polyethylene. The(1 0 0) [0 0 1] texture has been interpreted as being due to the principal slip plane in polyethylene being the (1 0 0) plane [7, 8]. But as was discussed by Gerrits and Young [17], a (1 0 0) [0 0 1] texture can be generated by either single slip or cross slip on planes which are combinations of (1 1 0), (1 $\bar{1}$ 0) and (1 0 0) planes. If slip could also take place on (0 1 0) planes a fibre texture would develop on constrained uniaxial drawing of polyethylene. Several reasons can be put forward to explain slip not taking place on (0 1 0) planes. For (0 1 0) [1 0 0] transverse slip to take place by movement of screw dislocations a relatively high energy is required as shown by Shadrake and Guiu [18]. Furthermore the absence of (0 1 0) fold planes restricts the (0 1 0) [1 0 0] transverse slip process and consequently it is thought to limit any type of slip on (0 1 0) planes.

Because for $\lambda \geq 3$ the lamellar normals are inclined by more than 45° with respect to the applied force, the shear stresses will generate a displacement perpendicular to the lamellar normals rather than a rotation of the normals towards the draw direction. Owing to this movement, the lamellae lock each other and further deformation is limited. The observations that the normals to the lamellae are inclined at approximately 65° to the draw direction can be explained by a limitation of crystal break-up during uniaxial drawing of melt-crystallized UHMW-PE. The process of crystal break up or coarse slip enables rotation of the lamellar crystals so that their normals become parallel to the draw direction. This coarse slip process is thought to be strongly influenced by the structure of the fold planes, in particular where re-entry is adjacent or random. If the slip planes for coarse slip are regular fold planes then large displacement of crystal blocks can occur without introducing constraints by the folds as shown in Fig. 5b. In specimens with an irregular fold-plane structure, coarse slip will be severely restricted due to the fact that the stems are accommodated in different planes, as schematically illustrated in Fig. 5d.

It is clear from the results presented above that the fold plane structure (lamellar structure) affects the solid-state drawability of UHMW-PE, and more specifically the rotation of the normals to the lamellar crystals towards the draw direction. This fold plane structure is predominantly determined by the crystallization conditions and hence it is not surprising that ultra-drawability generated by swelling above the dissolution temperature can also be lost by heating for a short period of time above the melting temperature [14].

5. Conclusions

The maximum solid-state drawability of melt-crystallized UHMW-PE is five. A × 5 drawn tape possesses a (1 0 0) [0 0 1] texture generated by transverse and chain slip processes. The lamellar normals are inclined at 65° with respect to the draw direction due to fold-plane restraints preventing lamellae from breaking up by coarse slip and rotating with their normals parallel to the draw direction. Further deformation of this type of texture will cause only shearing of the lamellae in the plane perpendicular to the lamellar normals. Hence, it is postulated that the drawability of melt-crystallized UHMW-PE is limited by fold plane restraints rather than entanglements.

Acknowledgements

The authors thank Professor R. J. Young and Professor P. J. Lemstra for valuable discussions, and they are grateful to DSM Research for making it possible to publish this work.

References

1. F. C. FRANK, A. KELLER and A. O' CONNOR, *Phil. Mag.* **3** (1958) 64.
2. A. PETERLIN and R. CORNELIUSSEN, *J. Polym. Sci. Polym. Phys. Ed.* **6** (1968) 1273.
3. K. ISHIKAWA, K. MIYASAKA and M. MAEDA, *ibid.* **7** (1969) 2029.
4. G. MEINEL, N. MOROSOFF and A. PETERLIN, *ibid.* **8** (1970) 1723.
5. G. MEINEL and A. PETERLIN, *ibid.* **9** (1971) 67.
6. A. PETERLIN, *J. Mater. Sci.* **6** (1971) 490.
7. O. YODA and I. KURIYAMA, *J. Polym. Sci. Polym. Phys. Ed.* **15** (1977) 773.
8. A. KAITO, K. NAKAYAMA and H. KANETSUNA, *J. Appl. Polym. Sci.* **28** (1983) 1207.
9. *Idem, ibid.* **30** (1985) 4591.
10. N. A. J. M. VAN AERLE and A. W. M. BRAAM, *Makromol. Chem.* **189** (1988) 1569.
11. T. KANAMOTO, A. TSURUTA, K. TANAKA, M. TAKEDA and R. S. PORTER, *Macromol.* **21** (1988) 470.
12. N. A. J. M. VAN AERLE and A. W. M. BRAAM, *J. Mater. Sci.* **23** (1988) 4429.
13. P. SMITH, P. J. LEMSTRA and H. C. BOOIJ, *J. Polym. Sci. Polym. Phys. Ed.* **19** (1981) 877.
14. P. J. LEMSTRA, N. A. J. M. VAN AERLE and C. W. M. BASTIAANSEN, *Polym. J.* **19** (1987) 85.
15. H. P. KLUG and L. E. ALEXANDER, "X-ray Diffraction Methods in Polymer Science" (Wiley, London, 1969).
16. D. T. GRUBB, J. DLUGOSZ and A. KELLER, *J. Mater. Sci. Lett.* **10** (1975) 1826.
17. N. S. J. A. GERRITS and R. J. YOUNG, *J. Mater. Sci.* **26** (1991) 2137.
18. L. G. SHADRAKE and F. GUIU, *Phil. Mag.* **34** (1976) 565.

Received 10 January
and accepted 7 June 1991